Featured Article

Drug Elimination Kinetics Following Subconjunctival Injection Using Dynamic Contrast-Enhanced Magnetic Resonance Imaging

Stephanie H. Kim,[1,2,4] **Karl G. Csaky,**[3] **Nam Sun Wang,**[1] **and Robert J. Lutz**[2]

Purpose. To determine the elimination rates of subconjunctivally injected model drugs using dynamic contrast-enhanced magnetic resonance imaging (DCE-MRI).

Methods. Gadolinium-diethylenetriaminopentaacetic acid (Gd-DTPA) and gadolinium-albumin (Gd-albumin) were injected in rabbits. Experiments were performed *in vivo* and *post mortem* and injection volumes of 200 and 600 μl were administered. Signal intensity values from MR images were converted to concentration of contrast agent to determine the mass clearance rates from subconjunctival space.

Results. Injection volume did not have a significant effect on clearance rate for both Gd-DTPA and Gd-albumin. The clearance rate of Gd-DTPA *in vivo* was about nine times faster than that *post mortem*. The *in vivo* and *post mortem* clearance rates of Gd-albumin were not significantly different. The *in vivo* half-life of Gd-DTPA was about 22 min while that of Gd-albumin was about 5.3 h.

Conclusions. DCE-MRI was used to quantitatively compare the subconjunctival clearance rates of Gd-DTPA and Gd-albumin. Dynamic clearance mechanisms present *in vivo* significantly reduced the subconjunctival concentration of Gd-DTPA but not Gd-albumin. Lymphatic clearance does not seem to be as significant as clearance by blood, as evidenced by data from Gd-albumin injections. Larger injection volumes may allow for longer retention times and prolonged release of drug.

KEY WORDS: drug transport barrier; magnetic resonance imaging; ocular pharmacokinetics; subconjunctival injection; transscleral drug delivery.

INTRODUCTION

Subconjunctival injections are routinely performed in patients to administer drugs such as corticosteroids (1) and antibiotics (2) for ocular treatment. Drug solutions injected into the subconjunctival space form a localized depot, which may allow for long-term sustained delivery. After subconjunctival injection, drugs penetrate the eye directly through the underlying tissues (3) and therapeutic concentrations can be achieved in the vitreous (4). While subconjunctival injections are commonly performed, the retention time of drug and the rate of drug elimination from the depot are unknown and have not been investigated in detail.

Fluorescence, autoradiography and drug extraction from tissues are traditional techniques used to study drug penetration and elimination in the eye. (3,5–7) However, methods which require data measurement from tissues *ex vivo* may not yield accurate results as the spatial distribution of drugs may change during the time interval that tissues are being harvested. The need to sacrifice multiple animals at various time points also renders these techniques inefficient for serial time studies.

Previous methods of examining the change in drug levels in the subconjunctival space after injection include extracting drug from the excised depot (8) and using a scintillation counter to measure the rate of loss of gamma-emitting materials (9). Drug extractions are inefficient since they require the use of multiple animals and it is also difficult to successfully remove the entire depot for analysis. The measurement of gamma-emitting compounds can give quantitative results *in vivo* but lacks information on spatial distribution. Magnetic resonance imaging has recently been introduced as a non-invasive approach to assess the subconjunctival delivery of ionic permeants (10). The study by Li *et al* analyzed concentration levels of Mn^{2+} and $MnEDTA^{2-}$ in the anterior chamber, posterior chamber, and the vitreous to assess the permeation and clearance of model ionic permeants. In our study, we measured the concentration levels of model drugs injected into the subconjunctival space using three-dimensional DCE-MRI. The rate of drug clearance was determined by following the concentration changes of the injected contrast agent from the local depot.

DCE-MRI was previously shown to be a useful tool for obtaining information regarding the spatial and temporal distribution of drugs *in vivo* (11). In ocular research, DCE-MRI has become a valuable method in the study of the

[1] Department of Chemical and Biomolecular Engineering, University of Maryland, College Park, Maryland, USA.
[2] National Institute of Biomedical Imaging and Bioengineering, National Institutes of Health, Bethesda, Maryland, USA.
[3] National Eye Institute, National Institutes of Health, Bethesda, Maryland, USA.
[4] To whom correspondence should be addressed. (e-mail:kimstep@mail.nih.gov)

integrity and permeability of the blood–retinal barrier ([12–14]). Ocular pharmacokinetic data have also been acquired with DCE-MRI by using a calibration curve to convert T_1 or signal intensity values to the concentration of the contrast agent ([15,16]).

Recent studies have demonstrated that elimination mechanisms present *in vivo* such as conjunctival lymphatic clearance and blood flow can significantly reduce the penetration of drugs to the vitreous ([16]) and anterior chamber ([10]) after transscleral delivery. The effect of dynamic clearance mechanisms on drug concentration levels in the subconjunctival space was studied by performing experiments *in vivo* and *post mortem*. Two different contrast agents, Gd-DTPA (590 Da) and Gd-albumin (67.5 kDa), were used as model drugs to understand the effect of molecular weight on clearance rate. The effect of injection volume was also studied by administering two different volumes (200 and 600 μl) of contrast agent.

MATERIALS AND METHODS

Animal Setup

Female New Zealand White rabbits weighing 3–3.5 kg were purchased from Covance Laboratories, Inc. (Vienna, VA, USA) and were used according to the guidelines set forth in the ARVO statement for the Use of Animals in Ophthalmic and Vision Research. Rabbits were intubated and inhalational isoflurane (1.5–2%) was administered through the endotracheal tube. Pulse and oxygenation, temperature, end-tidal CO_2 and respiratory rate were monitored during the entire MRI scan period. Proparacaine 1% ophthalmic drops (Allergan America, Hormigueros, PR) were used topically on the eye. The superonasal quadrant was exposed by placing a 9-0 vicryl suture at the limbus and rotating the eye downward. A 24 gauge × 3/4 in. long intravenous catheter (Terumo Medical Corporation, Somerset, NJ) was prepared as described in a previous study ([17]). The catheter was inserted and held in place by a puncture through the eyelid and advanced at least 5 mm superonasally under the conjunctiva. The needle was carefully withdrawn, leaving the tip of the catheter under conjunctival tissue. The eyelids were closed with tissue adhesive (Vetbond, 3 M Animal Care Products, St. Paul, MN) and the tip of the catheter was joined to a 7 m silicone/PE-10 tubing by a friction fit ([17]). Prior to connecting the catheter, the tubing was prefilled with either Gd-DTPA (Magnevist; Berlex, Inc., Monteville, NJ) diluted to 1 mM in phosphate buffered saline (PBS; pH 7.4) or Gd-albumin (Galbuim, Biopal, Inc., Worcester, MA) diluted to 0.1 mM protein in PBS. The contrast solution was faintly colored with 100 mg/mL sodium fluorescein (Akorn, Inc., Decatur, IL) to a final concentration of 0.5 mg/mL to enhance visibility of the fluid in the tubing. The bolus was administered after the rabbit was placed into the magnet and preliminary scans were acquired. The contrast solution was injected outside the scan room through a 1 mL syringe joined to the tubing with a 30 gauge needle.

MRI Experiment

Experiments were performed using a 4.7 Tesla MRI system (Bruker Instruments, Billerica, MA). 2 mL glass vials filled with PBS and the injection contrast solution were taped over the eye as reference standards. The rabbit was placed on a cradle and the entire head inserted in a volume coil. T_1-weighted images were acquired using a 3D gradient echo sequence. The sequence parameters were: TR/TE=40/5 ms, field of view (FOV)=9 cm×4.59 cm×9 cm, matrix=256×128×128, pulse angle 30° and averages = 1. The FOV was positioned to capture both eyes and the standard solution and the pixel resolution was 0.703 mm×0.179 mm×0.703 mm. One scan was acquired before bolus injection with each scan lasting 11 min. After injection, scans were acquired in continuous succession for at least 3 h for 200 μl injections and 5 h for 600 μl injections. Rabbits used for *post mortem* experiments were euthanized by pentobarbital overdose (200–250 mg/kg) within one hour prior to the start of the scan. All experiments were repeated at least in triplicate.

Image Analysis

MR images were analyzed using a program written in MATLAB (Mathworks, Natick, MA) designed to read and display Bruker file images. To convert signal intensities into concentration values of Gd-DTPA or Gd-albumin, a signal intensity *vs.* concentration calibration curve was constructed as described in previous studies ([17,18]) using samples of varying concentrations of contrast agent in PBS. Since injections were performed using large solution volumes and most of the subconjunctival bleb consisted of fluid, PBS was assumed to adequately model the fluid-filled tissue. The calibration curve was constructed by scanning the PBS samples using the same MR imaging parameters used for the rabbit experiments.

To obtain concentration values of the contrast agent in the subconjunctival space after injection, the entire 3D image set was normalized to the signal intensity of the contrast agent standard at each time point. The images were set to a threshold signal intensity level equivalent to a concentration of 0.01 mM for Gd-DTPA and 0.005 mM for Gd-albumin (detection limit).

Mass balance analysis was performed on individual slices which were all taken from one of the three dimensions. The in-plane resolution of the images used in analysis was 0.703×0.179 mm. For each slice that contained visible pixels in the subconjunctival space after thresholding, a region-of-interest (ROI) was manually drawn around the hyperintense bleb. The signal intensity of each pixel in the ROI was converted to a concentration of Gd-DTPA or Gd-albumin using the signal intensity *vs.* concentration calibration curve. After converting the signal intensity value to concentration for each pixel in the ROI, the mass of contrast agent in each pixel was computed by multiplying the pixel volume (0.088 mm^3) by concentration. By taking the sum of the mass of contrast agent in each slice, the total mass of contrast agent in the subconjunctival space was computed for each time point. The number of pixels that were included in each ROI was also recorded and multiplied by the pixel volume to obtain the total volume occupied by the contrast agent in the
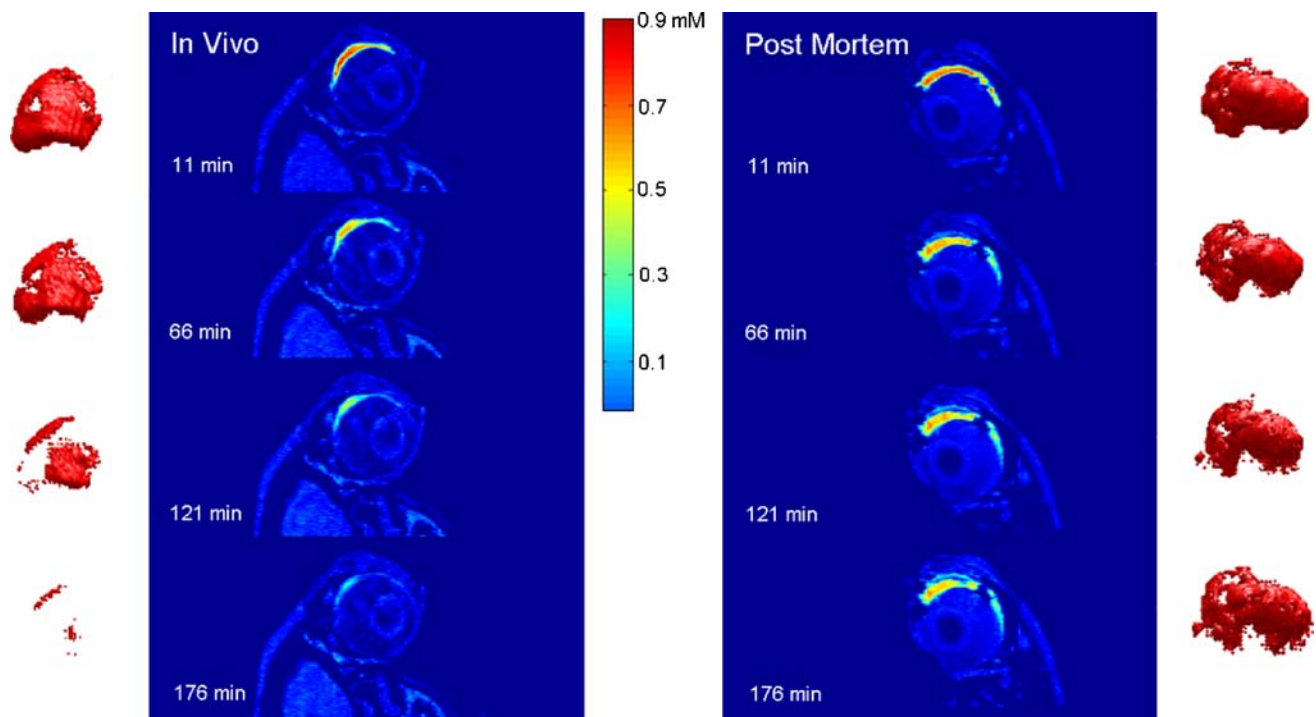
Fig. 1. Images acquired during *in vivo* and *post mortem* experiments after 200 μl Gd-DTPA injection. Times indicate minutes after injection. The volume occupied by Gd-DTPA is also shown in *red* by 3-dimensional reconstruction.

subconjunctival space at each time point. The average concentration of contrast agent in the subconjunctival space was calculated by dividing the total mass by the total volume.

The mass clearance data was fit to an exponential function, $M = Ae^{-kt}$, where M is the total mass of contrast agent in the subconjunctival space at time t, A is a constant, and k is the rate constant for clearance. Regressions were performed using Microsoft Excel (Microsoft Corporation, Redmond, WA) on semi-log plots of M *vs.* time, and values

of k were computed from each experiment. The half-life was derived from the rate constant ($t_{1/2}=0.693/k$).

RESULTS

Figures 1 and 2 show serial images acquired immediately after a 200 μl and 600 μl subconjunctival injection of Gd-DTPA, respectively. The images show a comparison of the *in vivo* and *post mortem* scans. The color bar indicates the
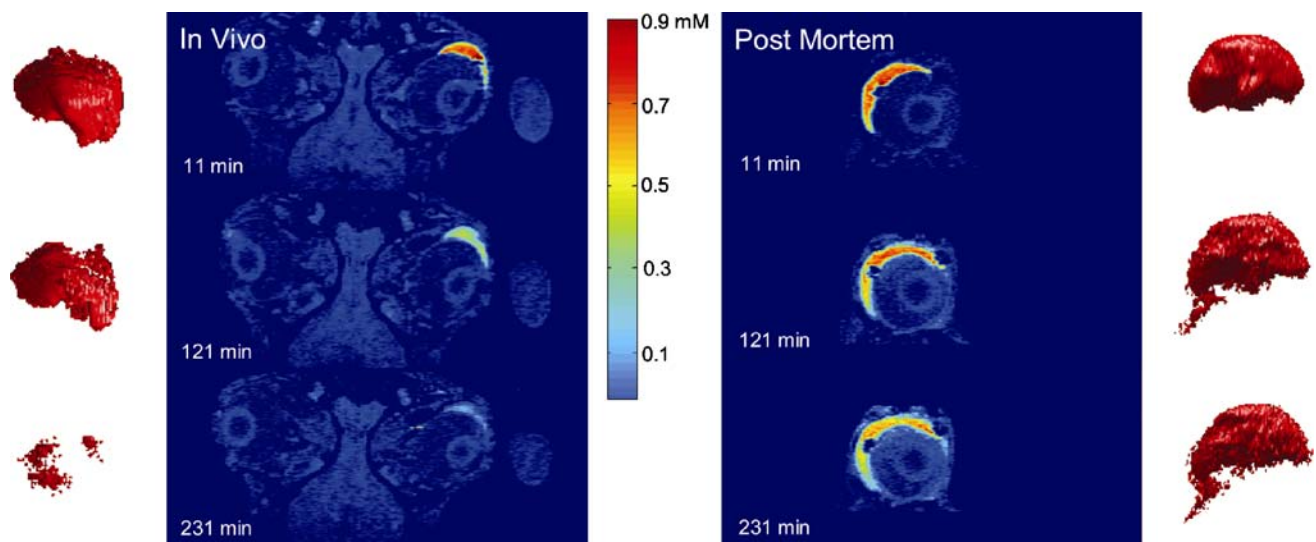

Fig. 2. Images acquired during *in vivo* and *post mortem* experiments after 600 μl Gd-DTPA injection. Times indicate minutes after injection. The volume occupied by Gd-DTPA is also shown in *red* by 3-dimensional reconstruction.

concentration of Gd-DTPA determined after conversion from signal intensity. Immediately after injection, the Gd-DTPA solution appears as a localized depot in the subconjunctival space at a high concentration. Over time, the concentration of Gd-DTPA in the subconjunctival bleb decreases dramatically *in vivo* for both injection volumes. About 3 h post-injection of 200 μl and 4 h post-injection of 600 μl, most of the Gd-DTPA molecules have disappeared from the depot *in vivo*. However, in the *post mortem* case for both injection volumes, the Gd-DTPA concentration decrease is not nearly as significant.

The Gd-DTPA mass clearance data for 200 and 600 μl injection experiments is plotted in Fig. 3A (*in vivo*) and B (*post mortem*). The plots also show the regression lines for the exponential fit of the mass data. The slopes of the regressions are given as average mass clearance rates (k) in Table I. While the k value for the 600 μl injection data appears to be less than the k value for the 200 μl data, the results from a one-tailed Mann–Whitney U test reveals that this difference is not significant for $p=0.05$ in both the *in vivo* and *post mortem* studies. The k values for 200 and 600 μl injections of Gd-albumin are also similar, and are not statistically different.

Figures 1 and 2 also present three-dimensional visual reconstructions of the apparent volume of Gd-DTPA, which were created by merging the slices that crossed through the subconjunctival bleb. These reconstructions are shown adjacent to the MR images at each respective time point. The apparent subconjunctival volume occupied by Gd-DTPA decreases dramatically *in vivo* while the *post mortem* scans show a slight increase in volume. This effect is also shown in Fig. 3C and D which are plots of the apparent Gd-DTPA volume in the subconjunctival space. Figure 3E and F are plots of the average concentration of Gd-DTPA in the subconjunctival space. They show a decrease in average concentration for all experiments.

MR images from 200 μl injections of Gd-albumin are shown in Fig. 4. A comparison of the *in vivo* Gd-albumin images in Fig. 4 to the *in vivo* Gd-DTPA images in Fig. 1 for the 200 μl injection volume indicates that the concentration of Gd-albumin decreases more slowly with time compared to Gd-DTPA. This observation is further substantiated by the quantitative representation of mass clearance given in Fig. 5A (DTPA) and B (albumin). The average *in vivo* half-life of Gd-DTPA is 22 min and of Gd-albumin is 5.3 h, as presented in Table I. Figure 5A and B also show that the *post mortem* decline of Gd-albumin concentration is about four times slower than the *post mortem* decline of Gd-DTPA for the 200 μl injection experiments, as evidenced by the calculated half-lives which are given in Table I.

The mass clearance data in Fig. 5B shows a slightly faster decrease of Gd-albumin *in vivo* compared to Gd-albumin

post mortem. Table I gives the respective half-lives as 5.3 h *in vivo* and 12.8 h *post mortem*. However, a one-tailed Mann–Whitney U test ($p=0.05$) suggests that the difference between the *in vivo* and *post mortem* clearance rates is not significant for Gd-albumin.

The apparent volume of Gd-albumin shows a slight increase *post mortem* (Fig. 5D). A similar effect is seen in Fig. 5C for the volume of Gd-DTPA *post mortem*. The *in vivo* volume of Gd-DTPA shows a considerable decrease, whereas that of Gd-albumin is less prominent. The faster decrease in volume of Gd-DTPA may reflect the higher clearance rate of Gd-DTPA than Gd-albumin from the subconjunctival space, since the volume decrease is due to the reduction in the number of pixels with signal intensities above the threshold.

Figure 5E and F show a decrease in average concentration of Gd-albumin in the subconjunctival space for all experiments. This trend also correlates with the images shown in Fig. 4, which show a slight decrease in the overall concentration of Gd-albumin.

DISCUSSION

Our study gives a quantitative comparison of the clearance of Gd-DTPA and Gd-albumin following subconjunctival injection in rabbits. The clearance rates of Gd-DTPA and Gd-albumin were determined by measuring the changes in signal intensity by means of DCE-MRI and converting these values into mass.

Results from *in vivo* experiments show that the mass decrease of Gd-DTPA is faster compared to that *post mortem*. This indicates that there are dynamic clearance mechanisms that are present *in vivo* but not *post mortem*. *In vivo*, drugs can be cleared from the subconjunctival depot by diffusion into surrounding tissues and also by entering lymphatic and blood vessels located in the conjunctiva (16, 19). *Post mortem*, drug elimination from the depot occurs mainly by diffusion since blood and lymphatic flow are presumed absent. While the clearance rate of Gd-DTPA *in vivo* was substantially higher than that *post mortem*, the *in vivo* and *post mortem* clearance rates of Gd-albumin did not differ significantly. This indicates that *in vivo* clearance mechanisms such as blood and lymph flow have a considerable effect on the elimination of Gd-DTPA but not on Gd-albumin.

Gd-DTPA molecules are smaller (<1 nm) and lower in molecular weight than Gd-albumin (4 nm). Drug absorption after subcutaneous injection has been shown to decrease linearly with increasing molecular weight (20), and a similar dependence may exist after subconjunctival injection. The disposition of nanoparticles following subconjunctival injection has been shown to display a size-dependence, with smaller particles reaching undetectable levels in the perioc-

Table I. Summary of Average Rate Constants Acquired *In Vivo* and *Post Mortem*

Contrast Agent, Injected Volume	k (*In Vivo*) (min^{-1})	Half-life (hrs)	k (*Post Mortem*) (min^{-1})	Half-life (hrs)
Gd-DTPA, 200 μl	0.0317	0.36	0.0035	3.3
Gd-DTPA, 600 μl	0.0247	0.47	0.0028	4.1
Gd-albumin, 200 μl	0.0022	5.3	0.0009	12.8
Gd-albumin, 600 μl	0.0018	6.4	–	–

In Vivo

Post Mortem
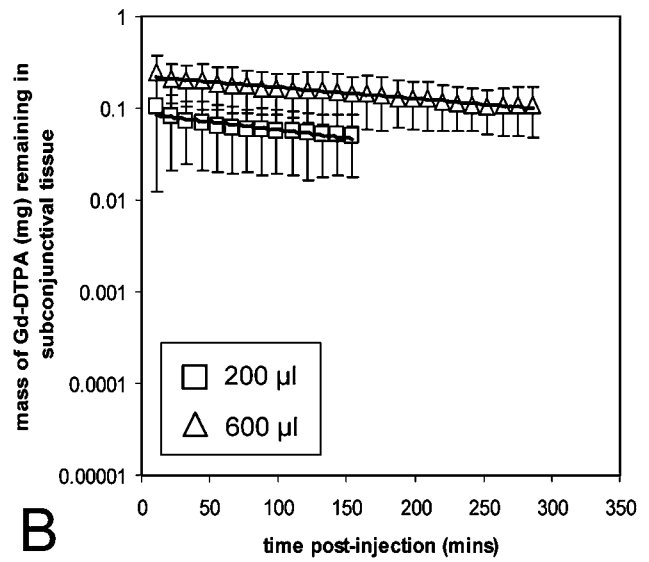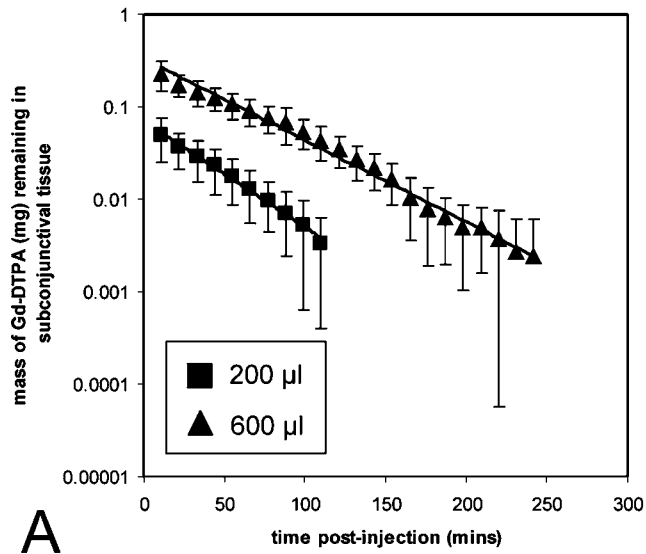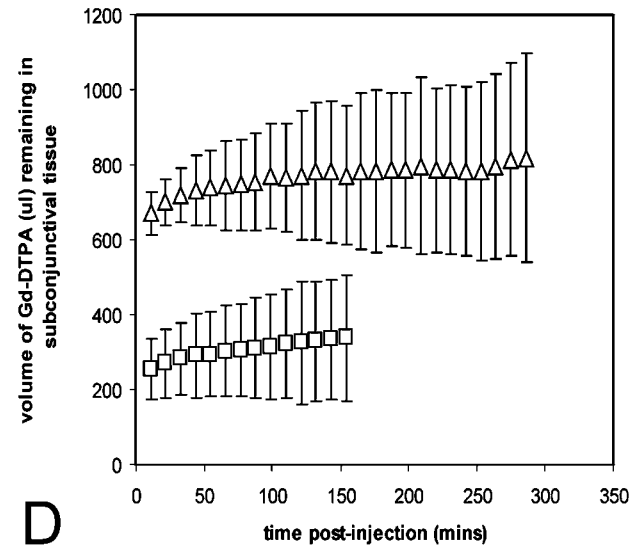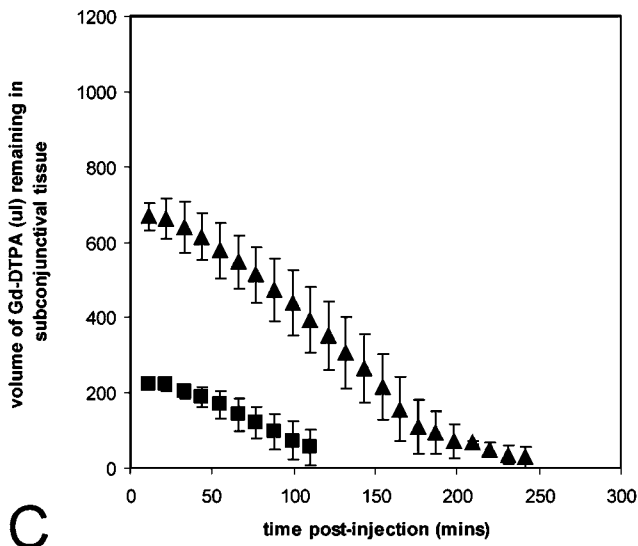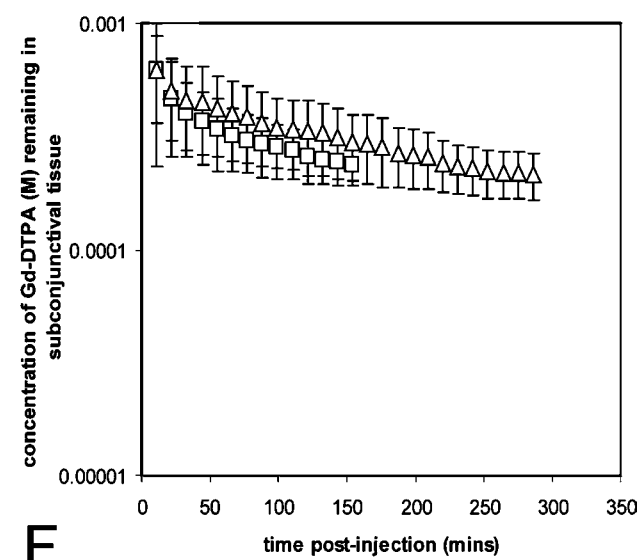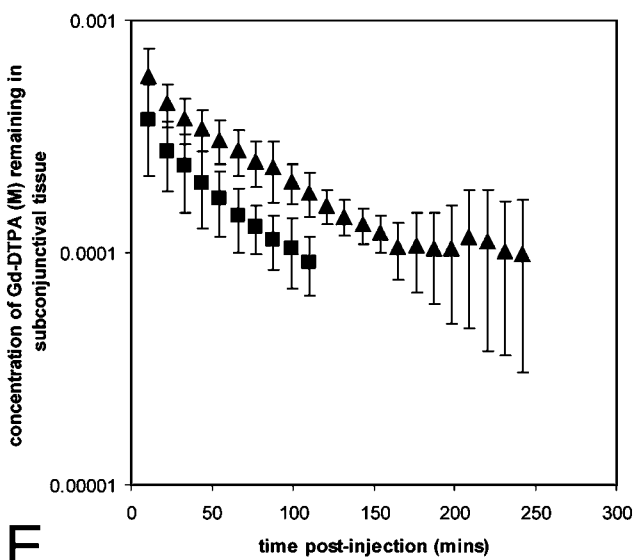
ular tissue while larger particles were almost entirely retained (21). Small drug molecules (<1 kDa) are thought to be preferentially absorbed by the blood capillaries while proteins larger than about 16 kDa are taken up primarily by the lymphatic system (20,22). The large molecular radius of Gd-albumin may hinder its entry into blood vessels so that clearance by blood flow is negligible. However, lymphatic vessels permit the entry of large particles and Gd-albumin may be cleared by the lymphatics present in the conjunctiva. Since albumin molecules are able to gain rapid access to lymphatic vessels but not to blood vessels, they are used in lymphatic flow studies which require administration by subcutaneous injection (Schornack, PA *et al. Proc Intl Soc Mag Reson Med,* ISMRM, 2001;58) (23,24). Gd-DTPA, on the other hand, should be easily cleared by both blood and lymphatics because of its small size. Our results show that the *in vivo* Gd-albumin clearance rate from the subconjunctival space was significantly slower than Gd-DTPA clearance rate by a factor of about 14, as seen from the values in Table I. These results may be indicative of the selective clearance of Gd-albumin through lymphatic vessels and the relatively low flow rate of lymph compared to that of blood (22). Our results also show that the clearance rates of Gd-albumin *in vivo* and *post mortem* are not significantly different. If Gd-albumin is cleared mostly by lymph and not by blood flow, this may suggest that lymphatic clearance after subconjunctival injection is not significant.

With the cessation of blood or lymph flow in the *post mortem* animal, a nearly zero clearance rate for both Gd-DTPA and Gd-albumin is expected. In our study, the *post mortem* decrease in mass is most likely due to the diffusion of contrast agent molecules out of the subconjunctival space. As molecules diffuse away from the subconjunctival depot, they will begin to fill the pixels that lie on the periphery of the injection site. But many of these pixels will have very low concentrations of contrast agent and will remain below the threshold value (0.01 mM for Gd-DTPA and 0.005 mM for Gd-albumin). Although these pixels contain contrast agent molecules, they are removed during image analysis. Therefore, the total mass of contrast agent decreases over time because molecules are continuously moving from high to low concentration areas, increasing the number of molecules residing in pixels that fall below the threshold. Since the diffusion of Gd-DTPA is faster than Gd-albumin, the *post mortem* "clearance" of Gd-DTPA is also faster than that of Gd-albumin.

On the other hand, the apparent volume was reported to increase in *post mortem* experiments. As molecules diffuse out of the depot, more molecules will enter the pixels surrounding the injection site. This will increase the concentration of contrast agent and in some cases the increase may be sufficient for pixels to have values above the threshold. These pixels are then counted as part of the subconjunctival depot during image analysis, and the volume will increase with time.

The volume measured in our studies represents the apparent volume of contrast agent in the eye, not the volume of the subconjunctival bleb. The changes in volume and mass of subconjunctival fluid may be different from that of the contrast agent. While fluid clearance may affect solute clearance, the technique used in our study cannot distinguish between fluid and solute clearance, and other measurement methods are necessary to explore these mechanisms in detail.

Maurice and Ota previously reported on the kinetics of subconjunctival injections in 1978 (9). They reported that the half-life of [22]Na was 9 min while that of albumin was 9 h. Our data shows that the half-life of Gd-DTPA after a 200 µl injection *in vivo* is about 22 min, which based on its molecular size, fits reasonably with Maurice and Ota's findings. The half-life of Gd-albumin reported in our study (5.3 h) also compares to the half-life of 9 h reported by Maurice and Ota. The discrepancy may be explained by the difference in data acquisition, as Maurice and Ota measured radioactive-labeled albumin from sections of
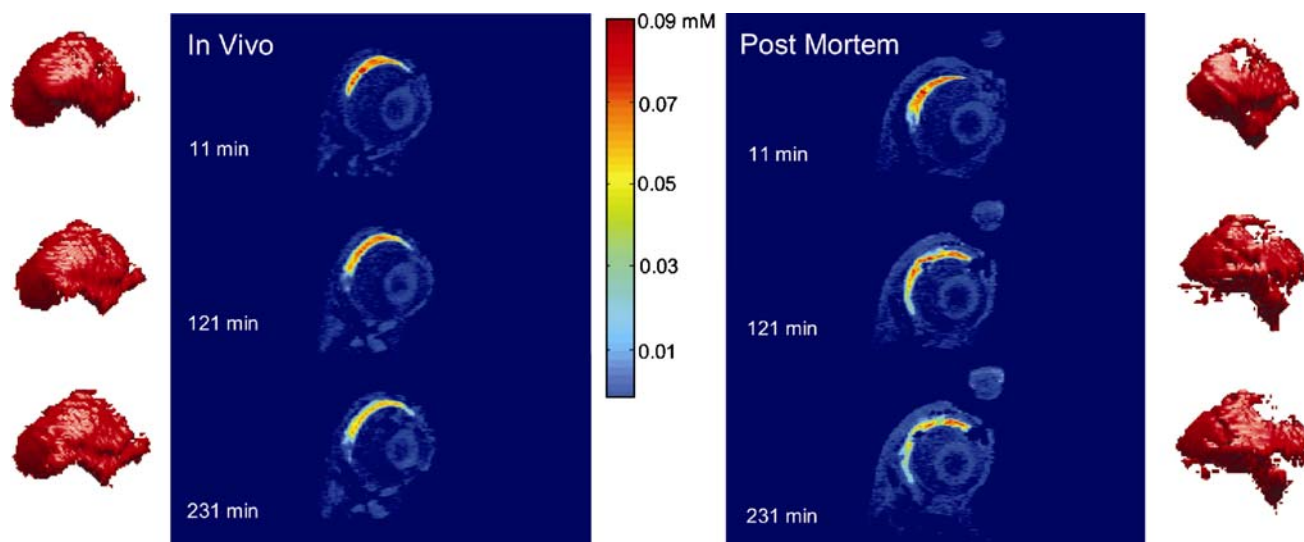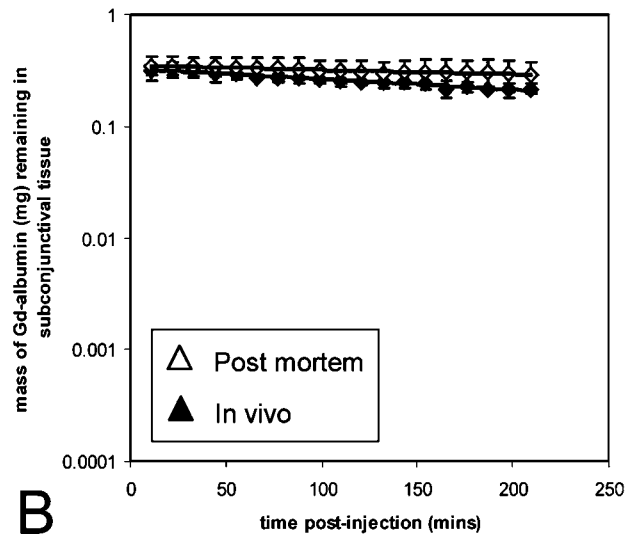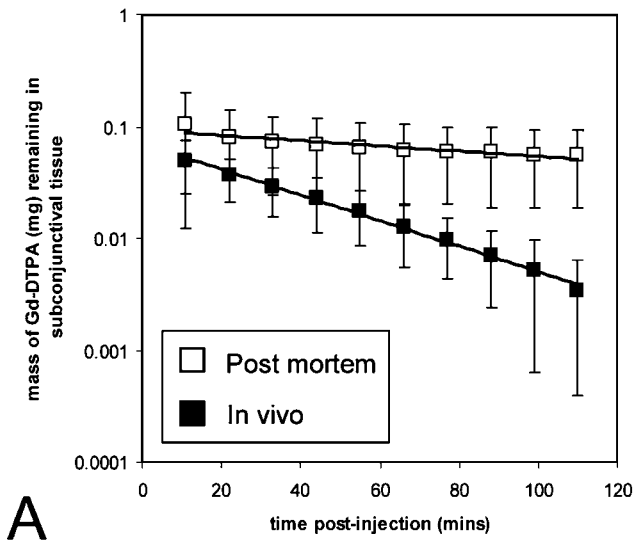

Fig. 4. Images acquired during *in vivo* and *post mortem* experiments after 200 µl Gd-albumin injection. Times indicate minutes after injection. The volume occupied by Gd-albumin is also shown in *red* by 3-dimensional reconstruction.
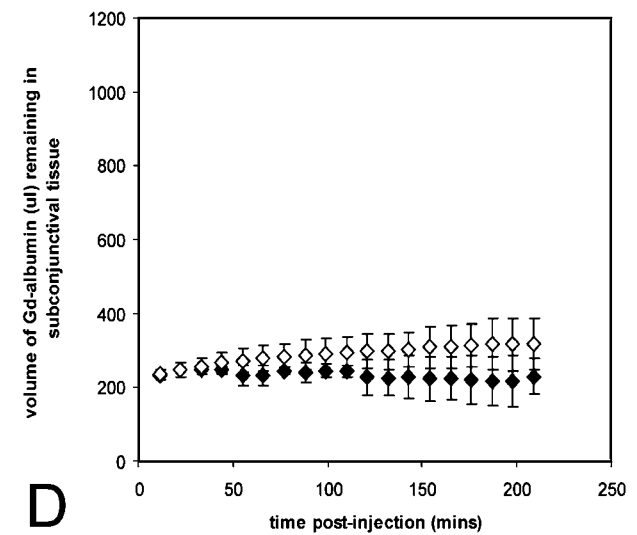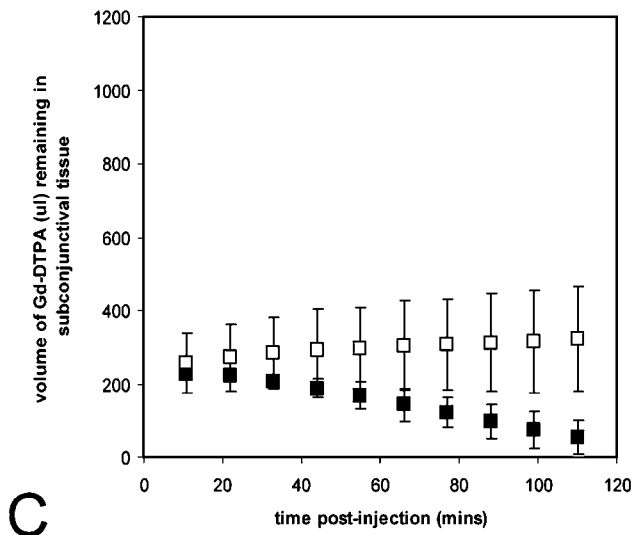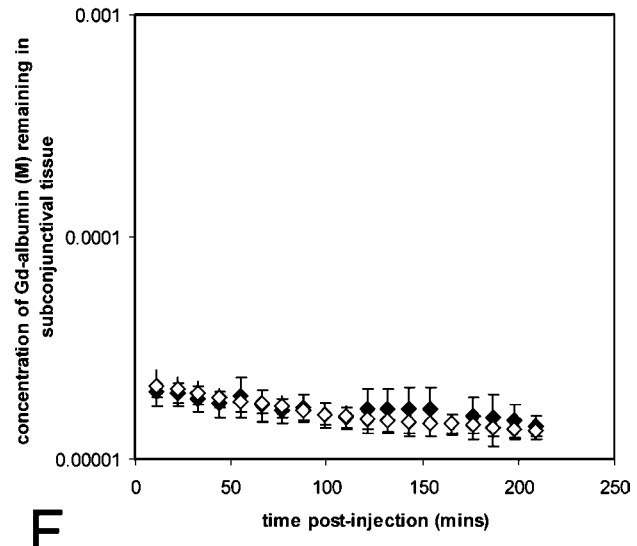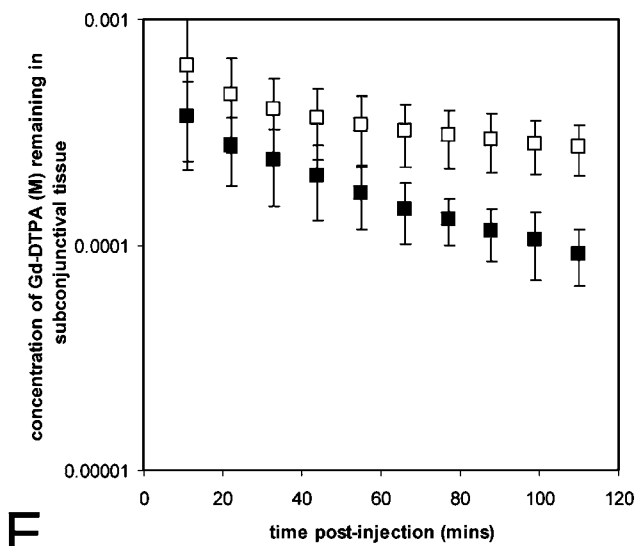
Gd-DTPA

Gd-albumin

◄ **Fig. 5.** Gd-DTPA (A, C, E) and Gd-albumin (B, D, F) change in mass, apparent volume and concentration after 200 μ1 subconjunctival injection *in vivo* and *post mortem*. Values are given as mean ± SD. *Lines* indicate regression for mass clearance data. r^2 values: ■=0.99, □=0.84, ◆=0.94, ◇=0.97.

excised tissue from enucleated eyes. For comparison to other tissues, Pain *et al* (25) reported a 3.6 h half-life for the clearance of albumin from subcutaneous injections in healthy human volunteers. Their clearance data showed a single exponential decay over times up to three hours.

Our results also showed that there was no significant difference in clearance rate between the 200 and 600 μl injection volumes. Previous studies using intramuscular injections reported a higher rate of absorption of hydrophilic drugs when the compounds were administered in smaller injection volumes (26,27). This is expected as a high interface area to injection volume ratio increases the drug absorption rate (28,29). However, in our study, the Mann–Whitney U test results determined that the clearance rates of 200 and 600 μl injections did not differ significantly. This may be due to a significant range in *k* values obtained for each volume, caused by variability in depot shape and size. The surface area to volume ratio also may not be significantly different for 200 and 600 μl injections because of the bleb shape, and a smaller volume may need to be tested.

While injection volume may not affect the rate of clearance, the larger volume injection did allow for longer retention times of contrast agent in the subconjunctival space. A comparison of mass values after 200 and 600 μl injections shows that there are higher amounts of Gd-DTPA in the subconjunctival space after the 600 μl injection at any given time point. This may be of clinical importance when longer retention times of drugs are required in the subconjunctival space to produce prolonged release of drug.

There are several limitations of the DCE-MRI technique used in our study. The concentration range of contrast agent detected by our DCE-MRI method is only about 2 log units. The effect of dose on clearance rate could not be studied due to the narrow concentration detection range. Concentration changes occurring beyond this range are undetectable with our technique and more sensitive methods such as measurement of T_1 may be required. The differences in relaxation times of PBS and subconjunctival tissue may contribute to error in the conversion of signal intensity to concentration, because our calibration was based on PBS and not on subconjunctival tissue. However, since the subconjunctival bleb is comprised mostly of fluid and not tissue, we assumed that PBS would adequately model the subconjunctival bleb. Also, our choice of Gd-DTPA as a low molecular weight model drug may not be fully adequate since Gd-DTPA is a hydrophilic molecule and may exhibit pharmacokinetic behavior that is different from lipophilic drugs. In following animal care and use guidelines, inhalational isoflurane was required to maintain general anesthesia. Clearance rates may be different in an anesthetized *vs.* a non-anesthetized animal, as the effect of inhalational isoflurane on blood and lymphatic flow in the eye is unknown.

Other non-invasive pharmacokinetic imaging tools besides MRI include PET and SPECT (30–32). These nuclear imaging techniques have been widely used to assess the distribution of radiolabeled drugs in various applications such as the determination of pharmacokinetics of anticancer therapies (33) and drugs for pulmonary delivery (34). The increased utilization of non-invasive pharmacokinetic imaging tools may enable better understanding of drug clearance and distribution in future drug delivery studies for the eye.

CONCLUSION

DCE-MRI is a useful technique that allows non-invasive *in vivo* data measurement in real-time. Our study demonstrates that sufficient spatial and temporal resolution can be achieved with DCE-MRI to capture the kinetic changes of subconjunctival drug clearance. DCE-MRI also enables the quantitation of data through the conversion of signal intensity to concentration. Results from subconjunctival injections of Gd-DTPA and Gd-albumin indicate that active clearance mechanisms (such as lymphatic and blood flow) can affect drug elimination rates. Lymphatic clearance does not seem to be as significant as clearance by blood, as evidenced by data from Gd-albumin injections. Injection volume (in the range of 200–600 μl) does not significantly alter clearance rate, but higher injection volumes allow for longer retention times of drug.

REFERENCES

1. P. A. Gaudio. A review of evidence guiding the use of corticosteroids in the treatment of intraocular inflammation. *Ocul. Immunol. Inflamm.* **12**:169–192 (2004).
2. R. J. Morris, D. McLeod, and Z. J. Gregor. Subconjunctival injections of antibiotics are used increasingly at the conclusion of intraocular and extraocular procedures. *Eye* **3** (Pt 6): 860–861 (1989).
3. H. J. McCartney, I. O. Drysdale, A. G. Gornall, and P. K. Basu. An autoradiographic study of the penetration of subconjunctivally injected hydrocortisone into the normal and inflamed rabbit eye. *Invest. Ophthalmol.* **4**:297–302 (1965).
4. O. Weijtens, E. J. Feron, R. C. Schoemaker, A. F. Cohen, E. G. Lentjes, F. P. Romijn, and J. C. van Meurs. High concentration of dexamethasone in aqueous and vitreous after subconjunctival injection. *Am. J. Ophthalmol.* **128**:192–197 (1999).
5. M. Barza, A. Kane, and J. L. Baum. Regional differences in ocular concentration of gentamicin after subconjunctival and retrobulbar injection in the rabbit. *Am. J. Ophthalmol.* **83**:407–413 (1977).
6. A. Tsuji, I. Tamai, and K. Sasaki. Intraocular penetration kinetics of prednisolone after subconjunctival injection in rabbits. *Ophthalmic Res.* **20**:31–43 (1988).
7. T. W. Kim, J. D. Lindsey, M. Aihara, T. L. Anthony, and R. N. Weinreb. Intraocular distribution of 70-kDa dextran after subconjunctival injection in mice. *Invest. Ophthalmol. Vis. Sci.* **43**:1809–1816 (2002).
8. P. H. Kalina, J. C. Erie, and L. Rosenbaum. Biochemical quantification of triamcinolone in subconjunctival depots. *Arch. Ophthalmol.* **113**:867–869 (1995).
9. D. M. Maurice and Y. Ota. The kinetics of subconjunctival injections. *Jpn. J. Ophthalmol.* **22**:95–100 (1978).

10. S. K. Li, S. A. Molokhia, and E. K. Jeong. Assessment of subconjunctival delivery with model ionic permeants and magnetic resonance imaging. *Pharm. Res.* **21**:2175–2184 (2004).

11. B. Reisfeld, S. Blackband, V. Calhoun, S. Grossman, S. Eller, and K. Leong. The use of magnetic resonance imaging to track controlled drug release and transport in the brain. *Magn. Reson. Imaging* **11**:247–252 (1993).

12. B. A. Berkowitz, Y. Sato, C. A. Wilson, and E. de Juan. Blood–retinal barrier breakdown investigated by real-time magnetic resonance imaging after gadolinium-diethylenetriaminepentaacetic acid injection. *Invest. Ophthalmol. Vis. Sci.* **32**:2854–2860 (1991).

13. E. L. Arrindell, J. C. Wu, M. D. Wolf, S. Nanda, D. P. Han, E. C. Wong, G. W. Abrams, W. F. Mieler, and J. S. Hyde. High-resolution magnetic resonance imaging evaluation of blood–retinal barrier integrity following transscleral diode laser treatment *Arch. Ophthalmol.* **113**:96–102 (1995).

14. B. A. Berkowitz, R. Roberts, H. Luan, J. Peysakhov, X. Mao, and K. A. Thomas. Dynamic contrast-enhanced MRI measurements of passive permeability through blood retinal barrier in diabetic rats. *Invest. Ophthalmol. Vis. Sci.* **45**:2391–2398 (2004).

15. W. E. Plehwe, D. W. McRobbie, R. A. Lerski, and E. M. Kohner. Quantitative magnetic resonance imaging in assessment of the blood–retinal barrier. *Invest. Ophthalmol. Vis. Sci.* **29**:663–670 (1988).

16. H. Kim, M. R. Robinson, M. J. Lizak, G. Tansey, R. J. Lutz, P. Yuan, N. S. Wang, and K. G. Csaky. Controlled drug release from an ocular implant: an evaluation using dynamic three-dimensional magnetic resonance imaging. *Invest. Ophthalmol. Vis. Sci.* **45**:2722–2731 (2004).

17. S. H. Kim, C. J. Galban, R. J. Lutz, R. L. Dedrick, K. G. Csaky, M. J. Lizak, N. S. Wang, G. Tansey, and M. R. Robinson. Assessment of subconjunctival and intrascleral drug delivery to the posterior segment using dynamic contrast-enhanced magnetic resonance imaging. *Invest. Ophthalmol. Vis. Sci.* **48**:808–814 (2007).

18. H. Kim, M. J. Lizak, G. Tansey, K. G. Csaky, M. R. Robinson, P. Yuan, N. S. Wang, and R. J. Lutz. Study of ocular transport of drugs released from an intravitreal implant using magnetic resonance imaging. *Ann. Biomed. Eng.* **33**:150–164 (2005).

19. M. R. Robinson, S. S. Lee, H. Kim, S. Kim, R. J. Lutz, C. Galban, P. M. Bungay, P. Yuan, N. S. Wang, J. Kim, and K. G. Csaky. A rabbit model for assessing the ocular barriers to the transscleral delivery of triamcinolone acetonide. *Exp. Eye Res.* **82**:479–487 (2006).

20. A. Supersaxo, W. R. Hein, and H. Steffen. Effect of molecular weight on the lymphatic absorption of water-soluble compounds following subcutaneous administration. *Pharm. Res.* **7**:167–169 (1990).

21. A. C. Amrite and U. B. Kompella. Size-dependent disposition of nanoparticles and microparticles following subconjunctival administration. *J. Pharm. Pharmacol.* **57**:1555–1563 (2005).

22. D. N. McLennan, C. J. H. Porter, and S. A. Charman. Subcutaneous drug delivery and the role of the lymphatics. *Drug Discov Today: Technologies* **2**:89 (2005).

23. L. D. Samuels. Lymphoscintigraphy. *Lymphology* **20**:4–9 (1987).

24. M. K. Nawaz, M. M. Hamad, H. M. Abdel-Dayem, S. Sadek, and B. G. Eklof. Tc-99m human serum albumin lymphoscintigraphy in lymphedema of the lower extremities. *Clin. Nucl. Med.* **15**:794–799 (1990).

25. S. J. Pain, R. S. Nicholas, R. W. Barber, J. R. Ballinger, A. D. Purushotham, P. S. Mortimer, and A. M. Peters. Quantification of lymphatic function for investigation of lymphedema: depot clearance and rate of appearance of soluble macromolecules in blood. *J. Nucl. Med.* **43**:318–324 (2002).

26. G. F. Warner, E. L. Dobson, N. Pace, M. E. Johnston, and C. R. Finney. Studies of human peripheral blood flow; the effect of injection volume on the intramuscular radiosodium clearance rate. *Circulation* **8**:732–734 (1953).

27. R. B. Sund and J. Schou. The determination of absorption rates from rat muscles: An experimental approach to kinetic descriptions. *Acta. Pharm Toxicol. (Copenh)* **21**:313–325 (1964).

28. J. Blaser, H. L. Rieder, and R. Luthy. Interface-area-to-volume ratio of interstitial fluid in humans determined by pharmacokinetic analysis of netilmicin in small and large skin blisters. *Antimicrob. Agents Chemother.* **35**:837–839 (1991).

29. K. Hirano, T. Ichihashi, and H. Yamada. Studies on the absorption of practically water-insoluble drugs following injection V: Subcutaneous absorption in rats from solutions in water immiscible oils. *J. Pharm. Sci.* **71**:495–500 (1982).

30. A. J. Fischman, N. M. Alpert, J. W. Babich, and R. H. Rubin. The role of positron emission tomography in pharmacokinetic analysis. *Drug. Metab. Rev.* **29**:923–956 (1997).

31. S. R. Cherry. Fundamentals of positron emission tomography and applications in preclinical drug development. *J. Clin. Pharmacol.* **41**:482–491 (2001).

32. O. Langer and M. Muller. Methods to assess tissue-specific distribution and metabolism of drugs. *Curr. Drug Metab.* **5**:463–481 (2004).

33. R. Hustinx, S. L. Eck, and A. Alavi. Potential applications of PET imaging in developing novel cancer therapies. *J. Nucl. Med.* **40**:995–1002 (1999).

34. M. Dolovich and R. Labiris. Imaging drug delivery and drug responses in the lung. *Proc. Am. Thorac. Soc.* **1**:329–337 (2004).